Extremum Seeking Control for Model-Free Auto-Tuning of Powered Prosthetic Legs

Saurav Kumar[1,2], Alireza Mohammadi[4], David Quintero[2,3], Siavash Rezazadeh[2], Nicholas Gans[1] and Robert D. Gregg[2,3]

***Abstract*—This paper proposes an extremum seeking controller (ESC) for simultaneously tuning the feedback control gains of a knee-ankle powered prosthetic leg using continuous-phase controllers. Previously, the proportional gains of the continuous-phase controller for each joint were tuned manually by trial-and-error, which required several iterations to achieve a balance between the prosthetic leg tracking error performance and the user's comfort. In this paper, a convex objective function is developed that incorporates these two goals. We present a theoretical analysis demonstrating that the quasi-steady-state value of the objective function is independent of the controller damping gains. Furthermore, we prove the stability of error dynamics of continuous-phase controlled powered prosthetic leg along with ESC dynamics using averaging and singular perturbation tools. The developed cost function is then minimized by ESC in real-time to simultaneously tune the proportional gains of the knee and the ankle joints. The optimum of the objective function shifts at different walking speeds, and our algorithm is suitably fast to track these changes, providing real-time adaptation for different walking conditions. Benchtop and walking experiments verify the effectiveness of the proposed ESC across various walking speeds.**

***Index Terms*—Powered prostheses, legged locomotion, rehabilitation robotics, extremum seeking, virtual constraints.**

I. Introduction

STATE-OF-ART powered knee-ankle prostheses are often controlled using a predetermined set of joint impedance controllers [1]. In this approach, the gait cycle is typically divided into multiple (usually *four* or *five*) phases, and the transitions between different walking phases are governed by finite state machines [2]–[4]. Operation in each phase is governed with a unique controller [2], [3], [5]. The controller in each phase has at least three tunable impedance parameters of stiffness, viscosity, and equilibrium angle for each actuated joint. This results in dozens of impedance parameters and switching rules, which needs to be changed as activities change, such as walking at different speeds.

Automating the control parameter tuning process can greatly improve the patient experience by adapting to varying walking conditions encountered in daily life. Some notable progress has been made in real-time automatic selection of control parameters. In [6], [7], rule-based fuzzy logic inference schemes, which are based on subjects' walking data, were developed in order to automate the tuning process of the knee joint control parameters. As noted by the authors in [8], this approach relies heavily on the knowledge and the experience of the human experts to formulate fuzzy rules. Adaptive dynamic programming was then used in [8] to alleviate the need for a human expert and demonstrate simultaneous tuning of the knee joint impedance parameters in simulations. However, it is unclear whether either of these approaches can simultaneously tune the impedance parameters of multiple joints, where the dynamics of one joint affects the other. The presented results in [6], [7] are also limited to a single walking speed (0.6 ms^{-1}). Apart from tuning impedance control parameters in powered prostheses, efforts have been made in the field of exoskeletons to tune the ankle joint parameters in real-time in order to improve the metabolic cost of the subject [9]–[11]. However, using the metabolic cost as an objective function leads to very slow adaptation that typically requires an hour to find a local optimum. Also, it is unclear how the optimization time is affected with additional knee joint parameters. This slow process might not be applicable for adapting to real-time changes in behavior or environment. In addition, the measurement of metabolic cost requires off-board sensors, e.g., face masks, which might be obtrusive to the user. An alternative approach to impedance-based controllers for powered prostheses are continuous-phase control schemes, which are inspired from the virtual constraints framework for robotic locomotion control (see, e.g., [12]–[16]). Continuous-phase gaits are kinematic relationships between the prosthesis joint angles that are parameterized by a mechanical phasing variable and are enforced via feedback. The continuous-phase control schemes reduce the number of tunable parameters compared to an impedance-based controller. In [16], a continuous-phase control scheme was employed in the stance period while an impedance-based controller was employed in the swing period. This approach reduced the number of tunable parameters by half. In [17], [18], the number of tunable parameters were further reduced by dividing the gait cycle into stance and swing phases and using a single controller for each. A single continuous-phase controller was used throughout the gait cycle in [19], which further reduced the number of tunable parameters to *four*, i.e., the proportional derivative (PD) gains for the knee and the ankle joints. Recently, unified phase-based gaits have been successfully tested on amputees across speeds and inclines [20], [21].

Although the continuous-phase control schemes for pow-

[1]Department of Electrical Engineering, [2]Department of Bioengineering, [3]Department of Mechanical Engineering, University of Texas at Dallas, Richardson, TX 75080, USA. [4] Department of Electrical and Computer Engineering, University of Michigan- Dearborn, Dearborn, MI 48128, USA. {sauravk,alireza.mohammadi,rgregg}@ieee.org, {ngans, dxq130330, siavash.rezazadeh} @utdallas.edu

This material is based upon work supported by the National Science Foundation (NSF) under Grant No. 1728057 and National Institute of Child Health & Human Development of the NIH under Award No. DP2HD080349. Any opinions, findings, and conclusions or recommendations expressed in this material are those of the authors and do not necessarily reflect the views of the NIH. R. D. Gregg holds a Career Award at the Scientific Interface from the Burroughs Wellcome Fund.

ered prosthetic legs reduce the number of tunable control parameters, the tuning of these controllers is still carried out manually and may need to change across different activities, such as walking at different speeds. The problem of automatic real-time tuning of continuous-phase controllers for powered prosthetic legs remains an open problem. Although progress has been made in model-based adaptive control of biped robots [22], such *model-based* approaches, which rely on input-output feedback linearization, are difficult to use in powered prosthetic applications because of the need for expensive multi-axis load cells in order to measure the patient-prosthesis socket interaction forces [18].

In this paper, we present a methodology for automatic tuning of continuous-phase controllers for powered prosthetic legs using a perturbation-based extremum seeking control (ESC) scheme [23], [24]. ESC, being a model-free control method, requires neither the explicit knowledge of the powered prosthesis nor the patient wearing it. However, it requires an objective function that quantifies both the prosthetic leg's performance and the user's comfort. It is the first time in the literature that an objective function is being developed for real-time adaptation of a powered prosthetic leg to different walking conditions via ESC. Indeed, there has not been sufficient research on defining quantifiable objectives that can represent walking factors capable of improving the human-prosthesis interaction [25]. The objective functions (related to tracking error) proposed in [26] enjoy fast convergence to the optimum but do not consider the subject's discomfort. The use of metabolic cost as an objective function [9]–[11] provides a measure of the subject's discomfort but is too slow for real-time adaptation to changing behaviors. In our previous work [27], we developed a theoretical framework for designing ESC schemes to tune the PD gains of powered prosthesis controllers to reduce the tracking error. That work was limited to verifying the effectiveness of our algorithms in simulations (i.e., no experimental results) and made no consideration of the user's comfort, which is an important aspect in practical application. In this paper, we use ESC to *experimentally* perform simultaneous tuning of the proportional gains for the knee and ankle joints with fixed derivative gains. In particular, we extend the literature on auto-tuning of powered prosthetic legs in the following significant ways:

Contributions of this paper

(i) *Development of a convex objective function for powered prosthetic legs* - Based on our observations from extensive benchtop and walking experiments, we developed a convex objective function for continuous-phase control of powered prosthetic legs, which can be used at different walking speeds. In particular, the objective function in [27] has been modified to incorporate the patient's comfort level. The characteristic of the developed objective function is that its optimum varies across walking speeds.

(ii) *Simultaneous tuning of multiple joints across different walking speeds* - This paper experimentally verifies the effectiveness of ESC for tuning the proportional gains for a powered knee-ankle prostheses *across different walking speeds*. To the best of our knowledge, this is the first contribution towards demonstrating simultaneous adaptation of the proportional gains for both the knee and the ankle joints of a transfemoral powered prosthetic leg.

(iii) *Demonstrating that the quasi-steady-state value of the developed objective function is independent of the damping gains K_d* - We present a theoretical analysis for the closed-loop robot dynamics with the ESC, which demonstrates that the quasi-steady-state value of the objective function is independent of the damping gains. Changing the damping gains not only exacerbates the control due to noisy velocity measurements, but also, our analysis shows that tuning the damping gains does not necessarily improve the steady-state performance of the powered prosthetic leg. Finally, using tools from averaging and singular perturbation theory, we prove the stability of error dynamics of continuous-phase controlled powered prosthetic legs along with the ESC dynamics for tuning the proportional gains.

With respect to the automatically tuned impedance-based controllers in the literature, our adaptation algorithm enjoys a unique combination of several features. First, we demonstrate the effectiveness of our adaptation algorithm *across different walking speeds* as opposed to carrying out adaptation at a fixed walking speed [6], [7]. Our algorithm takes approximately one minute to track real-time changes in the optimal proportional gains, which is sufficiently fast compared to prior approaches that take 1-2 hours for adaptation [9]–[11]. Second, our ESC-based online adaptation scheme is capable of *simultaneously tuning* the proportional gains of continuous-phase controllers for *multiple* joints. Third, our optimization method only needs the onboard prosthetic leg sensors.

The rest of this paper is organized as follows. In Section II, we present the experimental setup, notion of continuous-phase control of powered prosthetic legs, and a brief review of the perturbation-based ESC framework that is used in this paper. Next, we develop a convex objective function for ESC in Section III based on fixed-gain benchtop and walking experiments with the prosthesis and present a theoretical analysis of the objective function along with the stability proof of the prosthetic leg's error dynamics with the ESC dynamics. Next, in Section IV we present the experimental results of the proposed approach implemented on the powered prosthetic leg, which was tested by an able-bodied human subject wearing a knee-bypass adapter as in [20]. We discuss these results in Section V and provide concluding remarks in Section VI.

II. Preliminaries

This section briefly presents the hardware setup, continuous-phase control of the powered knee-ankle prosthesis [19], [21], and the perturbation-based ESC [23].

A. Prosthetic Leg Embedded Systems and Sensing

The benchtop and walking experiments were performed on the UT Dallas powered knee-ankle prosthetic leg, which is shown in Fig. 1. A multi-stage transmission was developed in [20], [21] to actuate both the knee and ankle joints. The actuator consisted of a high-speed Maxon EC-4pole 30, 200

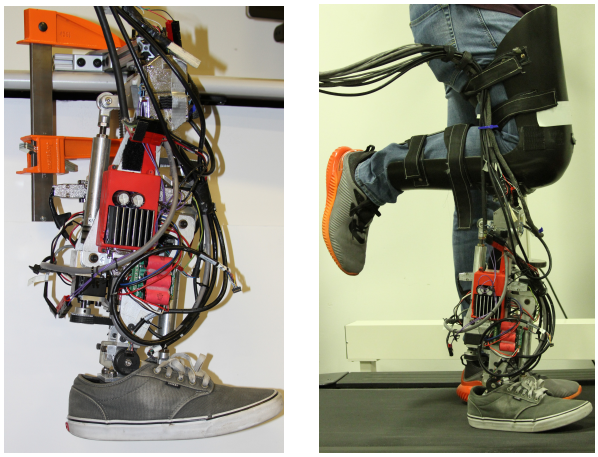

(a) Benchtop mode (b) Walking mode

Fig. 1: Different experimental setups: (a) In the benchtop mode, the top of the prosthetic leg knee joint was attached onto a rigid bench; (b) In the walking mode, an able-bodied subject walked on the prosthetic leg using a knee-bypass adapter.

Watt brushless direct current motor powered by a Elmo Gold Twitter R80/80 motor amplifier. The motor was connected to a timing belt drive with sprockets, giving a 4:1 reduction at the ankle and 2:1 at the knee. The sprockets were connected to a Nook 12 mm diameter, 2 mm lead ball screw connected to a lever arm that actuated the joints. The motor amplifiers were powered by an Agilent 6673A 35V/60A DC power supply.

A dSPACE DS1007 system with Freescale OorIQ P5020, 2 GHz processor was tethered to the prosthesis for control computation and data acquisition sampled at 1 kHz. US Digital EC35 encoders provided measurements of the joint angles. The joint velocities were numerically computed using a first-order Butterworth low-pass filter (LPF) at 8 Hz cutoff frequency. To measure the global thigh angle for the purpose of calculating the phase variable (Section II-B), a LORD Microstrain 3DMGX4-25 inertial measurement unit (IMU) was placed on top of the prosthetic knee joint. Further detail of the prosthesis design specifications can be found in [21].

B. Continuous-Phase Control of Powered Prosthetic Legs

In continuous-phase control for powered prostheses, the desired trajectory generation for the knee and ankle joints are synchronized to the thigh angle. This means that the evolution of the knee and the ankle joint trajectories are not parameterized by time, but rather by a monotonically increasing variable s_h (computed from the user's global thigh angle). This variable $s_h \in [0, 1)$ is called the phase variable, and its extreme values represent the start and the end of a gait cycle. At the end of a gait cycle, s_h is reset to 0. Thus, the phase variable parameterization of the desired trajectory allows synchronization of the prosthetic leg joint patterns to the phase of the user. The continuous-phase control of powered prosthetic legs includes:

*1) **Computation of phase variable [20], [21]:*** The phase variable s_h is computed online using measurements of the thigh angle from the IMU according to

$$s_h(\nu(t)) = \frac{\nu(t) - \nu^+}{\nu^- - \nu^+} \tag{1}$$

where "+" and "-" indicate the value of the phase angle ν at the start and the end of the gait cycle, respectively. The phase angle $\nu(t)$ is computed using the patient's thigh angular position $\phi(t)$ and its integral $\Phi(t) = \int_0^t \phi(\tau)d\tau$ as

$$\nu(t) = \text{atan2}\big((\Phi(t) + \Gamma)z, (\phi(t) + \gamma)\big) \tag{2}$$

where the constant parameters z, γ, and Γ represent an adaptable scaling factor, the thigh angle shift, and the thigh integral shift, respectively (see [21] for further details).

*2) **Phase-based generation of desired trajectories [19]–[21], [28]:*** Consider a desired joint trajectory expressed as a function of a phase variable. Let the discrete signal $x[n]$ represent this trajectory sampled over N evenly distributed points. The DFT is a linear transformation of the signal $x[n]$ that produces a sequence of complex numbers across a spectrum of discrete frequency components $X(k)$:

$$X(k) = \sum_{n=0}^{N-1} x[n] W_N^{kn}, \quad k = 0, 1, \dots K \tag{3}$$

where N is the finite number of samples, K is the running index for the finite sequence of k (up to $N-1$), and $W_N = e^{-j(2\pi/N)}$ is the complex quantity. Since $x[n]$ is periodic, there are a finite number of discrete frequency terms $X(k)$. After obtaining the frequency content terms $X(k)$, the original signal can be reconstructed using Fourier interpolation:

$$x[n] = \frac{1}{N} \sum_{k=0}^{K} X[k] W_N^{-kn}, \quad n = 0, 1, \dots, N-1 \tag{4}$$

where $X[k] = Re\{X[k]\} + jIm\{X[k]\}$ and $W_N^{-kn} = Re\{W_N^{-kn}\} + jIm\{W_N^{-kn}\}$ in standard complex form. Since the joint kinematic signals are real numbers, only the real part of $x[n]$ is taken into consideration. Equation (4) can then be decomposed as a summation of sinusoids using Euler's relationship $e^{j\Omega} = \cos\Omega \pm j\sin\Omega$, $\Omega \in \mathbb{R}$, for W_N within the DFT. From this we finally obtain the desired joint angle function

$$\begin{aligned} h^d(s_h) \;=\; & \frac{1}{2}\rho_0 + \frac{1}{2}\rho_{N/2}\cos(\pi N s_h) \\ & + \sum_{k=1}^{\frac{N}{2}-1} \Big[\rho_k \cos(\Omega_k s_h) - \psi_k \sin(\Omega_k s_h)\Big] \end{aligned} \tag{5}$$

where $\Omega_k = 2\pi k$, and ρ_k and ψ_k are the computed coefficients from the real and imaginary terms of $X[k]$ from (4).

*3) **Control Law:*** Continuous-phase controllers coordinate the knee and ankle patterns of the prosthetic leg by enforcing constraints that are parameterized by a common phasing variable [19], [21]. In particular, a continuous-phase gait encodes the desired motions of the actuated variables in the form of output functions

$$y = q - h^d(s_h) \tag{6}$$

where $y = [y_k \;\; y_a]^T \in \mathbb{R}^2$ is the tracking error, $q = [q_k \;\; q_a]^T \in \mathbb{R}^2$ is the measured angular position of joint i (with $i = k$ for the knee and $i = a$ for the ankle), and $h^d(\cdot) \in \mathbb{R}^2$

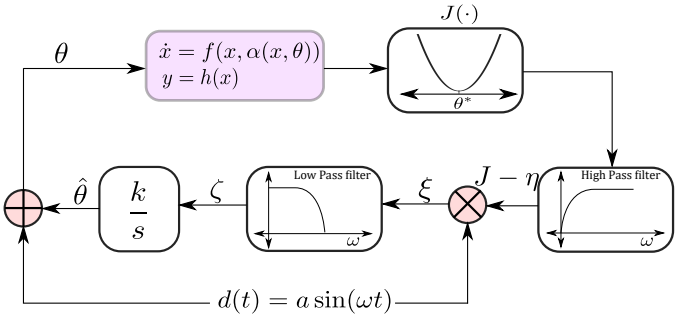

Fig. 2: Perturbation-based ESC block diagram.

is the desired periodic joint angle trajectory as a function of the normalized phase variable $s_h \in [0, 1)$.

In the continuous-phase approach [16], [20], [21], a model-free output PD control law of the form

$$u = -K_p y - K_d \dot{y} \tag{7}$$

is used to enforce the continuous-phase gait in (6). The proportional and the damping gains in (7) are given by

$$K_p = \begin{bmatrix} K_{p_k} & 0 \\ 0 & K_{p_a} \end{bmatrix} \; ; \; K_d = \begin{bmatrix} K_{d_k} & 0 \\ 0 & K_{d_a} \end{bmatrix} \tag{8}$$

where K_{p_i}, K_{d_i} are the proportional and the damping gains for the i^{th} joint, respectively. The control torque vector is given by $u = [u_k \; u_a]^T \in \mathbb{R}^2$, where u_k and u_a are the torques applied to the prosthetic knee and ankle joint, respectively. The permissible range of values for K_p and K_d were obtained in experiments by trial-and-error. In particular, for all values of $K_{p_k} \in [1.6, 7]$ and $K_{d_k} \in [0.1, 0.3]$, the knee joint dynamics were stable. Similarly, for all values of $K_{p_a} \in [4, 17]$ and $K_{d_a} \in [0.4, 1.5]$, the ankle joint dynamics were stable. The manual tuning procedure of PD gains for walking experiments using continuous-phase controllers was described in [21]. In practice, for a more compliant, smooth behavior of the knee joint, $\dot{y}_k$ was replaced with the measured angular velocity $\dot{q}_k$ in (7).

C. Perturbation-Based Extremum Seeking Algorithms

Consider a single-input single-output nonlinear control system

$$\dot{x} = f(x, u) \tag{9}$$
$$y = h(x) \tag{10}$$

where $x \in \mathbb{R}^n$ is the state vector, $y \in \mathbb{R}$ is the output, and the functions $f : \mathbb{R}^n \times \mathbb{R} \to \mathbb{R}^n$ and $h : \mathbb{R}^n \to \mathbb{R}$ are smooth. Given the state feedback control law $u = \alpha(x, \theta)$, parameterized by a tunable parameter θ, the closed-loop control system dynamics are given by

$$\dot{x} = f(x, \alpha(x, \theta)). \tag{11}$$

The objective of ESC is to maximize/minimize, in real-time, a suitably defined objective function $J(\cdot)$ at the steady-state for the closed-loop dynamics trajectories without knowing *a priori* the extremum θ^* of the objective function $J(\cdot)$.

A well-known extremum seeking algorithm, due to Krstic et al. [23], [24] is the perturbation-based ESC, whose basic architecture is depicted in Fig. 2. The signal $d(t) = a\sin(\omega t)$, which is called the *dither signal*, is a periodic perturbation signal that is added to the current best estimate of the parameter θ, which is denoted by $\hat{\theta}$. Taking θ as input, the objective function $J(\cdot)$ generates the output, which is passed through a high pass filter (HPF) that removes the DC component, η, to give $J - \eta$. The output of the HPF is demodulated by using the same dither signal $d(t)$. The resulting demodulated signal, denoted by ξ, is then passed through a LPF that generates the output ζ, which is proportional to the gradient of the current measured output $J(\cdot)$. Next, the signal $\zeta(t)$ is passed through an integrator with gain k to give $\hat{\theta}$. The sign of the integrator gain k should be chosen such that the inequality $kJ'' < 0$ holds.

In the extremum seeking literature [24], [29], [30], the following assumptions are typically made regarding the control system dynamics and the convex objective function: (i) the closed loop dynamics are much faster than the extremum seeking adaptation dynamics and the system (11) is locally exponentially stable for every $\theta \in I$, where I is an interval consisting the range of stable controller parameters; (ii) there exists a unique optimum θ, denoted by θ^*, of the convex objective function $J(\cdot)$. Considering the first order LPF and HPF with cut-off frequencies, ω_l and ω_h, respectively, the ESC dynamics can be written as

$$\dot{\hat{\theta}} = k\xi \tag{12}$$
$$\dot{\xi} = -\omega_l \xi + \omega_l (J - \eta) a\sin(\omega t) \tag{13}$$
$$\dot{\eta} = \omega_h (J - \eta). \tag{14}$$

The choice of ESC parameters, i.e., $a, \omega, k, \omega_h, \omega_l$, are critical to stable adaptation. These should be chosen such that a time scale separation between the plant and the ESC dynamics holds. For the powered prosthetic leg, the choice of ESC parameters are explained in detail in Appendix A. Additional details regarding ESC can be found in [23].

III. Development and Analysis of ESC on a Powered Prosthetic Leg

In this section, we describe the structure of ESC for powered prosthetic legs. Next, we explain the observations obtained from fixed-gain experiments, and then using these observations we develop a convex cost function for ESC. Finally, we present a theoretical analysis of the developed objective function and a stability proof of the error dynamics of a continuous-phase controlled powered prosthetic leg along with the ESC dynamics.

A. Structure of ESC for Powered Prosthetic Legs

The block diagram of the proposed automatically tuned controller is shown in Fig. 3. As it can be seen from Fig. 3, there are three main components: (i) a continuous-phase PD controller, denoted by Γ; (ii) ESC, whose operation mechanism has been explained in Section II-C and; (iii) the objective function block, denoted by $J(\cdot)$. In ESC, it is assumed that the system is operating at its steady-state. However, the error dynamics of a powered prosthetic leg are not steady-state

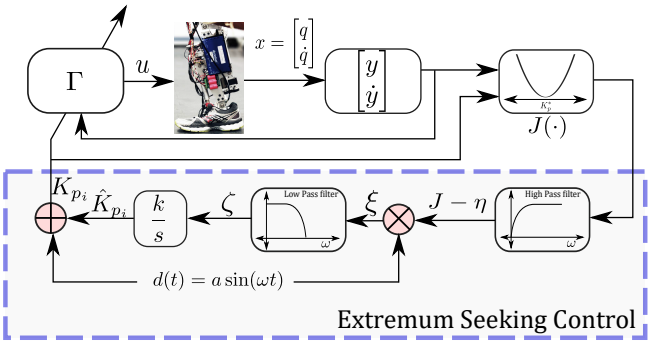

Fig. 3: Block diagram of the proposed automatically tuned controller. The controller Γ is a PD controller that drives y and $\dot{y}$ to zero. The controller parameter, K_{p_i} is automatically tuned by ESC in real-time such that the objective function in (16) is minimized.

during walking. In particular, it was observed in prior experiments that the ankle tracking error significantly increased during the terminal stance phase, i.e., ankle push-off phase. This is due to the fact that during the ankle push-off, the ankle actuator had to overcome the reaction torque from the subject's weight. Consequently, in order to employ perturbation-based ESC scheme proposed in [23], [29], the joint tracking error must pass through proper filters such that a steady-state value of the objective function can be achieved.

Obtaining a steady-state tracking error : Recently, a LPF was designed in [31] to perform ESC for a non-steady state output of the system. In order to generate an approximately steady-state ankle tracking error, we used a rate limiter, which limits the rate of change of the ankle joint tracking error. The rising and the falling rates were limited to 10 and -5 deg/sec, respectively and were chosen such that the rate of the dither signal was not limited. For instance, a dither signal with $a = 1, \omega = 0.2$ Hz has a maximum rise and fall rate of 0.8 and -0.8 deg/sec, respectively. We remark here that in order to produce a steady-state ankle joint tracking error profile, the saturation of the objective function, as in [32], was avoided here. This is because the saturation of the objective function could introduce additional tuning parameters, depending on the walking speed. Once the steady-state joint tracking error was obtained, it was used as an input to the amplitude detector, which is discussed in Section III-B.

B. Fixed-Gain Experiment Observations and Developing a Convex Cost Function

This section focuses on developing a convex ESC objective function with respect to the proportional gains through fixed-gain experiments on the powered prosthetic leg. We performed fixed-gain benchtop and walking experiments at different walking speeds to understand the behavior of the trajectory tracking error performance for different proportional gains. In the benchtop mode, the prosthetic leg knee joint was attached onto a rigid bench (see Fig. 1a) and the prosthetic leg joints were commanded time-based human knee and ankle trajectories [33]. To study the effect of the proportional gain of the knee controller K_{p_k} on the steady-state knee tracking error at a particular walking speed, the proportional gain of

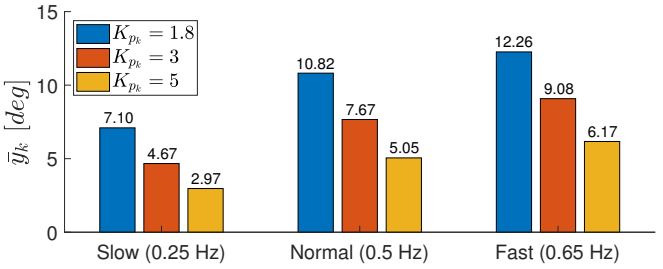

Fig. 4: Plot of averaged knee filtered tracking error for slow (0.25 Hz), normal (0.5 Hz) and fast (0.65 Hz) trajectories with varying proportional gain of the knee controller K_{p_k} in benchtop mode. The proportional gain of the ankle controller K_{p_a} was fixed at 10 for all the experiments.

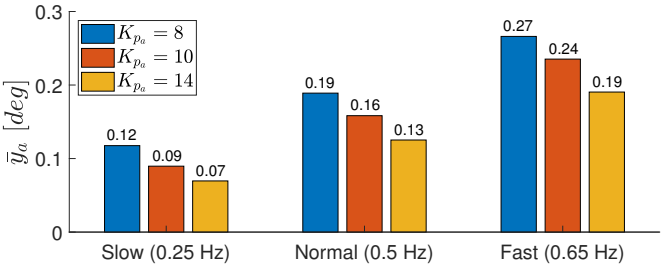

Fig. 5: Plot of averaged ankle filtered tracking errors for slow (0.25 Hz), normal (0.5 Hz) and fast (0.65 Hz) trajectories with varying proportional gain of the ankle controller K_{p_a} in benchtop mode. The proportional gain of the knee controller K_{p_k} was fixed at 3 for all the experiments.

the ankle controller K_{p_a} was fixed at 10 and K_{p_k} was varied in the following trials. The damping gains for both of the joints were fixed throughout the experiments at $K_{d_k} = 0.25$ and $K_{d_a} = 0.6$. Three different values of K_{p_k}, i.e., 1.8, 3, and 5 were tested each at slow, normal, and fast walking trajectories resulting in a total of 9 experiments. The slow, normal, and fast walking speeds were defined at 0.25, 0.5, and 0.65 Hz, respectively, in the benchtop mode. Similarly, in order to study the effect of K_{p_a} on the ankle tracking error, the same procedure was repeated with K_{p_k} fixed at 3 while different values of K_{p_a}, i.e., 8, 10, and 14, were tested in the subsequent experiments. Each experiment was run for 30 seconds, and the instantaneous joint tracking errors were recorded. In total, taking two joints into consideration, 18 fixed-gain benchtop experiments were performed.

In the walking mode, an able-bodied subject walked on the prosthetic leg using a knee-bypass adapter as in [20] (see Fig. 1b). The prosthetic leg joints were commanded to follow human trajectories based on the phase variable (see (1)). A similar procedure was followed to understand the effect of K_{p_k} and K_{p_a} on the joint tracking error, resulting in a total of 18 fixed-gain walking experiments. The slow, normal, and fast walking speeds were defined at 0.89, 1.12, and 1.34 metres/second (m/s). The protocol for walking experiments was approved by the Institutional Review Board (IRB) at the University of Texas at Dallas. To prevent fatigue, the subject was given sufficient rest in between the experiments. All the experiments were conducted on the same day and took three hours to complete them.

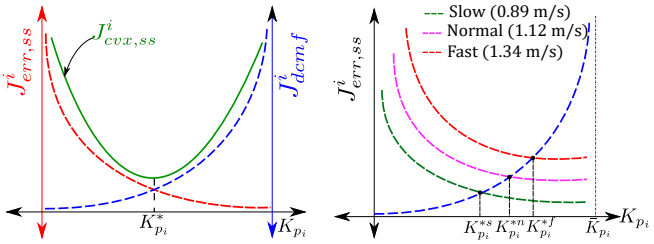

(a) Objective functions at fixed walking speed

(b) Objective functions at different walking speeds

Fig. 6: Illustrations of the objective functions from fixed-gain experiments. (a) Double plot of tracking error objective function, $J^i_{err,ss}$ on the left $y-$axis (shown in red) and discomfort objective function, J^i_{dcmf} on the right $y-$ axis (shown in blue) with respect to K_{p_i}. The green curve represents $J^i_{cvx,ss}$; (b) Plot of tracking error objective function, $J^i_{err,ss}$ for different walking speeds, indicating the presence of different optimums.

Figs. 4, 5 show the bar plots of averaged filtered knee and ankle tracking error, denoted by $\bar{y}_k$ and $\bar{y}_a$, respectively, in the benchtop mode. A similar trend was observed in the walking experiments and is therefore not shown here for brevity. With joint PD control action, the tracking error of the system reaches a limit cycle that is nearly sinusoidal of the form, $y_i(t) = y_0 + r_i \sin(\omega_0 t)$, where y_0, r_i, ω_0 are constants. In order to extract the amplitude of the limit cycle, r_i, we followed the method in [29]. It was noticed in the experiments that the DC component y_0 for both of the joints were approximately zero. Therefore, we concentrated on estimating the magnitude of the tracking error, e.g., r_i. To accomplish this, we used a first order HPF with a cut-off frequency $\Omega_h = 0.1$ Hz. The output of the HPF, $r_i \sin(\omega_0 t)$ is then squared to give $(r_i^2/2)(1 - \cos^2(\omega_0 t))$, which is then passed through an eighth order LPF with a cut-off frequency $\Omega_l = 0.35$ Hz to give $r_i^2/2$. This combination of the HPF, squaring and LPF, known as amplitude detector, obtained the amplitude of the limit cycle and eliminated the limit cycle frequency, ω_0 (here, cadence). The underlying assumption in designing a good amplitude detector was that $\omega_0 \gg \Omega_h, \Omega_l$ [29]. For our case, the walking frequency at slow and fast speed corresponded to walking at 0.45 and 0.65 Hz, respectively. However, since the walking frequency was very small, we used a high order analog LPF (eighth order) so that the walking frequency was mostly eliminated. We used the output of the LPF as the joint tracking error objective function at the steady-state, denoted $J^i_{err,ss}$. The average knee filtered tracking error, $\bar{y}_k$, is then obtained by taking the root mean of $J^k_{err,ss}$. We have the following two observations from these experiments:

1) For a particular speed, $\bar{y}_k$ decreases with the increase in the proportional gain of the knee controller K_{p_k}. This can be noticed by comparing the magnitudes of the bars in the individual bins in Fig. 4. Based on the first observation, the graph of $J^i_{err,ss}$ with respect to K_{p_i} for the i^{th} joint should look like the red dashed curve in Fig. 6a.
2) For a particular proportional gain of the knee controller K_{p_k}, $\bar{y}_k$ increases with the increase in the walking speed. This can be noticed by comparing the magnitudes of the same colored bars across different bins in Fig. 4. A similar trend of $J^i_{err,ss}$ with respect to K_{p_i} was noted at all the three walking speeds. However, based on the second observation, due to the difference in the magnitude of $J^i_{err,ss}$ for different walking speeds, the graph of $J^i_{err,ss}$ with respect to K_{p_i} should be shifted up for fast walking, as compared to slow walking and depicted in Fig. 6b.

The same observations held for the ankle joint as shown in Fig. 5. Based on the observations in Figs. 6a, 6b, we conclude that attempting to minimize $J^i_{err,ss}$ with respect to K_{p_i} would result in the highest allowable K_{p_i} for producing the best tracking performance. However, it was noted from fixed-gain experiments that the best tracking performance did not imply optimal performance of the prosthetic leg from the perspective of the subject. Due to the large inertia of the powered prosthesis and high K_{p_i}, the interaction with the subject would be too forceful and makes the subject feel less comfortable [21]. Therefore, in addition to $J^i_{err,ss}$, the objective function must also include a term that takes into account the subject's discomfort.

The comfort of the user can be effectively quantified by either measuring the socket interaction forces or by computing the joint jerks, i.e., the derivative of joint accelerations [34]. The socket interaction forces are expensive to measure [18] due to the need of expensive multi-axis load cells. Additionally, joint acceleration readings are extremely noisy, resulting in inaccurate information that cannot be used reliably in control implementation. On the other hand, we know from fixed-gain experiments that the proportional gain of the PD controller directly affects how forceful the leg interacts with the patient. The higher the proportional gains, the more forceful the prosthetic leg interacts with the patient, resulting in less comfort. Therefore, we accommodate the comfort of the user through the barrier-like function

$$J^i_{dcmf} = \frac{1}{(K_{p_i} - \bar{K}_{p_i})^2} \tag{15}$$

where $\bar{K}_{p_i}$ represents the upper bound of K_{p_i} for stable leg operation. It can be noticed that as K_{p_i} approaches $\bar{K}_{p_i}$ in (15), J^i_{dcmf} increases, thereby indicating a greater subject discomfort. The graph of J^i_{dcmf} with respect to K_{p_i} is depicted by the blue dashed curve in Figs. 6a and 6b. Thus, we conclude that, in order to provide the greatest user comfort, attempting to minimize J^i_{dcmf} with respect to K_{p_i} would result in lowest allowable K_{p_i}. However, as noted from the fixed-gain experiments, this would result in a worse tracking performance.

In order to have a balance between the tracking performance and the user's comfort, we propose the following convex sum

$$J^i_{cvx,ss} = w^i_{err} \cdot J^i_{err,ss} + w^i_{dcmf} \cdot J^i_{dcmf} \tag{16}$$

as the convex cost function at the steady-state, where w^i_{err} is the preference on the tracking error objective function and $w^i_{dcmf} = 1 - w^i_{err}$ is the preference on the user's discomfort objective function. The green curve in Fig. 6a indicates the shape of $J^i_{cvx,ss}$. To bring $J^i_{err,ss}$ and J^i_{dcmf} on the same scale, a suitable scaling factor for $J^i_{err,ss}$ was chosen. In particular,

the scaling factor for the knee and ankle were chosen as 0.01 and 1, respectively. Depending on the convex combination of the objective functions, $J^i_{err,ss}$ and J^i_{dcmf}, the optimum K_{p_i}, denoted by $K^*_{p_i}$, might move left or right in Fig. 6a. Also, based on the second observation, Fig. 6b shows that the intersection of $J^i_{err,ss}$ with J^i_{dcmf} produces different $K^*_{p_i}$ for different walking speed. This clearly indicates that $K^*_{p_i}$ changes with walking speeds. This means the prosthesis is more forceful only when the task demands it. The optimum K_{p_i} for slow, normal, and fast walking speeds are indicated by $K^{*s}_{p_i}, K^{*n}_{p_i}$, and $K^{*f}_{p_i}$ in Fig. 6b. Once the convex objective function in (16) is developed, the goal of ESC is to simultaneously tune K_{p_i} for the knee and the ankle joints by minimizing $J^i_{cvx,ss}$.

Remark 1: *In practice, since the comfort level can vary between different patients, the weights w^i_{err}, w^i_{dcmf} on the objective functions $J^i_{err,ss}, J^i_{dcmf}$ have to be tuned just once by a technician. Once the weights are chosen for the user based on their preference, ESC will automatically tune the proportional gains across different walking speeds.*

Remark 2: *Minimizing the objective function $J^i_{cvx,ss}$ in (16) can also be seen as a multi-objective optimization problem with fixed* a priori *weights. Therefore, multi-objective ESC techniques like [35], [36] could be used to automate the selection of a priori weights.*

C. Theoretical Analysis

The prosthetic leg knee and ankle dynamics are governed by [18]

$$M(q)\ddot{q} + C(q,\dot{q})\dot{q} + G(q) + E(q)^T\lambda = u + \tau_{\text{socket}} \tag{17}$$

where $M(q) \in \mathbb{R}^{2\times 2}$ is the mass matrix, $C(q,\dot{q}) \in \mathbb{R}^{2\times 2}$ is the matrix of Coriolis/centrifugal forces, $G(q) \in \mathbb{R}^{2\times 1}$ is the vector of gravitational forces, $E(q) \in \mathbb{R}^{c\times 2}$ is the Jacobian matrix associated with c physical constraints between the foot and the ground, and $\lambda \in \mathbb{R}^c$ is the Lagrange multiplier associated with the ground reaction force (GRF). An external torque τ_{socket} applied on the joints is due to the socket interaction forces exerted at the mid-thigh, which connects the prosthesis to the subject's residual limb.

First, we derive the tracking error dynamics for the prosthetic leg. By taking two derivatives of y along the vector field of (17), we have

$$\ddot{y} = \frac{d}{dt}\Big(\frac{\partial y}{\partial q}\dot{q}\Big) = A(q)u + N(q,\dot{q}) \tag{18}$$

where the matrix $A(q) = \dfrac{\partial y}{\partial q}M^{-1} \in \mathbb{R}^{2\times 2}$ is the *decoupling matrix* associated with the output y. Also,

$$N(q,\dot{q}) = \frac{d}{dt}\Big(\frac{\partial y}{\partial q}\Big)\dot{q} - \frac{\partial y}{\partial q}M^{-1}\big\{C(q,\dot{q})\dot{q} + G(q) + E(q)^T\lambda - \tau_{\text{socket}}\big\} \tag{19}$$

lumps the effect of the nonlinearities in (17). We make the following assumption, which is common in the robotics literature [18] and can be verified numerically:

Assumption 1: *The decoupling matrix $A(q)$ is non-singular and positive definite.*

We denote the estimates of the proportional gains in (8) by $\widehat{K}_p \in \mathbb{R}^2$ and add the dither signal

$$D_\omega(t) = \begin{bmatrix} a\sin(\omega_k t) & 0 \\ 0 & a\sin(\omega_a t)\end{bmatrix} \tag{20}$$

to the proportional gain estimates, i.e., $\widehat{K}_{p_k}$ and $\widehat{K}_{p_a}$, to obtain

$$K_p = \begin{bmatrix} \widehat{K}_{p_k} + a\sin(\omega_k t) & 0 \\ 0 & \widehat{K}_{p_a} + a\sin(\omega_a t)\end{bmatrix}. \tag{21}$$

Next, we substitute the PD control law (7) into (18) to get

$$\frac{d}{dt}\Big(\frac{\partial y}{\partial q}\dot{q}\Big) = -A(q)(K_p y + K_d\dot{y}) + N(q,\dot{q}). \tag{22}$$

Defining the new state $\tilde{x} := \begin{bmatrix} y \\ \dot{y}\end{bmatrix} = \begin{bmatrix} \tilde{x}_1 \\ \tilde{x}_2\end{bmatrix} \in \mathbb{R}^4$, the tracking error dynamics can be written as

$$\dot{\tilde{x}} = \tilde{A}(\tilde{x}, \widehat{K}_p)\tilde{x} + \widetilde{N}(q,\dot{q}) \tag{23}$$

where

$$\begin{aligned} \tilde{A}(\tilde{x}, \widehat{K}_p) &= \begin{bmatrix} 0_{2\times 2} & I_{2\times 2} \\ -A(q)(\widehat{K}_p + D_\omega(t)) & -A(q)K_d\end{bmatrix} \\ \widetilde{N}(q,\dot{q}) &= \begin{bmatrix} 0_{2\times 1} \\ N(q,\dot{q})\end{bmatrix}. \end{aligned} \tag{24}$$

To simplify the analysis, we neglect the HPF and the LPF dynamics in the ESC loop and consider a single integrator ESC dynamics as in [30]. The ESC dynamics for the estimate of proportional gain K_{p_i} for the i^{th} joint can be written as

$$\dot{\widehat{K}}_{p_i} = kaJ^i(\tilde{x}, \widehat{K}_{p_i} + a\sin(\omega_i t))\sin(\omega_i t). \tag{25}$$

Let $K^*_{p_i}$ denote the optimum proportional gain for the i^{th} joint. Denoting the estimation error of K_{p_i} by $\widetilde{K}_{p_i} = \widehat{K}_{p_i} - K^*_{p_i}$, the augmented closed-loop dynamical equations for the error dynamics are

$$\dot{\tilde{x}} = \tilde{A}(\tilde{x}, \widetilde{K}_p)\tilde{x} + \widetilde{N}(q,\dot{q}) \tag{26}$$

$$\dot{\widetilde{K}}_{p_i} = kaJ^i(\tilde{x}, \widetilde{K}_{p_i} + K^*_{p_i} + a\sin(\omega_i t))\sin(\omega_i t), \text{ for } i \in \{k, a\} \tag{27}$$

Remark 3: *We do not tune the damping gains K_d by ESC because once the fast tracking error dynamics settle down, the tuning of K_d will not effect the quasi-steady-state value of the objective function. The following result uses singular perturbation analysis to show that the quasi-steady-state of the objective function is independent of the damping gains K_d.*

Proposition 1: *Consider the prosthesis tracking error dynamics in (18) along with the ESC update laws in (25). Neglecting the filter dynamics[1] used in the amplitude detector, the objective function (16) can be written as*

$$J^i = w^i_{err}\|y\|^2 + w^i_{dcmf}\Big(\frac{1}{K_{p_i} - \bar{K}_{p_i}}\Big)^2 \tag{28}$$

In quasi-steady-state, the objective function for the i^{th} joint (28) is independent of K_{d_i}, where w^i_{err} and $w^i_{dcmf} = 1 - w^i_{err}$ are the weights on the error objective function and subject's discomfort objective function, respectively. In particular, the

[1]To simplify the analysis, it is a common practice to remove the filters used in the amplitude detector (see [29] for details).

quasi-steady-state value of the objective function in (28) is given by

$$J^i_{qs} = w^i_{err} \cdot \|(\widehat{K}_{p_i} + a\sin(\omega_i t))^{-1} A(q)^{-1} N(q,\dot{q})\|^2 + w^i_{dcmf} \cdot \frac{1}{(\widehat{K}_{p_i} + a\sin(\omega_i t) - \bar{K}_{p_i})^2}. \quad (29)$$

Proof. The stability of the error dynamics in (26)-(27) is analyzed by averaging and singular perturbation method [37]. To perform the singular perturbation analysis, we bring the closed-loop dynamics in (26)-(27) to a *standard* singular perturbation form. We perform the change of coordinates

$$z = \tilde{x} - \tilde{x}^* \quad (30)$$

where $\tilde{x}^*$ is the solution[2] to

$$\tilde{A}(\tilde{x}^*, \widetilde{K}_p)\tilde{x}^* + \widetilde{N}(q,\dot{q}) = 0. \quad (31)$$

Expressing the error dynamics given by (26) in terms of the new coordinates in (30), we get

$$\begin{aligned} \dot{z} &= \tilde{A}(z+\tilde{x}^*, \widetilde{K}_p)(z+\tilde{x}^*) + \widetilde{N}(q,\dot{q}) \quad (32)\\ &= \tilde{A}(z+\tilde{x}^*, \widetilde{K}_p)z + \widetilde{N}(q,\dot{q}) + \tilde{A}(z+\tilde{x}^*, \widetilde{K}_p)\tilde{x}^*. \end{aligned}$$

In the new coordinates $(z, \widetilde{K}_p)$, the origin $(z, \widetilde{K}_p) = (0,0)$ is an equilibrium point because

$$\dot{z} = \tilde{A}(\tilde{x}^*, 0)\underbrace{z}_{=0} + \underbrace{\widetilde{N}(q,\dot{q}) + \tilde{A}(\tilde{x}^*,0)\tilde{x}^*}_{=0} = 0. \quad (33)$$

The overall error dynamics in the new coordinates are

$$\Sigma' := \begin{cases} \dot{z} = \tilde{A}(z+\tilde{x}^*, \widetilde{K}_p)z + \widetilde{N}(q,\dot{q}) + \tilde{A}(z+\tilde{x}^*, \widetilde{K}_p)\tilde{x}^* \\ \dot{\widetilde{K}}_{p_i} = kaJ^i(z+\tilde{x}^*, \widetilde{K}_{p_i}+K^*_{p_i}+a\sin(\omega_i t))\sin(\omega_i t). \end{cases} \quad (34)$$

We define a slow time scale $\tau := \omega_i t$ and let $k := \omega_i \delta K$. Expressing (34) in the new time scale given by τ, we get

$$\begin{aligned} \omega_i \frac{dz}{d\tau} &= \tilde{A}(z+\tilde{x}^*, \widetilde{K}_p)z + \widetilde{N}(q,\dot{q}) + \tilde{A}(z+\tilde{x}^*, \widetilde{K}_p)\tilde{x}^* \\ \frac{d\widetilde{K}_{p_i}}{d\tau} &= \delta K a J^i(z+\tilde{x}^*, \widetilde{K}_{p_i} + K^*_{p_i} + a\sin\tau)\sin\tau. \quad (35) \end{aligned}$$

According to the singular perturbation theory, we first need to find the quasi-steady-state value of $z = [z_1\ z_2]^T$ in (35). Accordingly, we set $\omega_i = 0$, corresponding to instantaneous changes of the fast dynamics, and solve the resulting algebraic equations:

$$\tilde{A}(z+\tilde{x}^*, \widetilde{K}_p)z + \widetilde{N}(q,\dot{q}) + \tilde{A}(z+\tilde{x}^*, \widetilde{K}_p)\tilde{x}^* = 0. \quad (36)$$

Substituting $\tilde{A}(z+\tilde{x}^*, \widetilde{K}_p)$ and $\widetilde{N}(q,\dot{q})$ from (24) in (36), we have

$$\begin{bmatrix} 0_{2\times 2} & I_{2\times 2} \\ -A(q)(\widetilde{K}_p + K^*_p + D_\omega(\tau)) & -A(q)K_d \end{bmatrix} \begin{bmatrix} z_1 \\ z_2 \end{bmatrix} + \begin{bmatrix} 0_{2\times 1} \\ N(q,\dot{q}) \end{bmatrix} \quad (37)$$
$$+ \begin{bmatrix} 0_{2\times 2} & I_{2\times 2} \\ -A(q)(\widetilde{K}_p + K^*_p + D_\omega(\tau)) & -A(q)K_d \end{bmatrix} \begin{bmatrix} \tilde{x}^*_1 \\ \tilde{x}^*_2 \end{bmatrix} = \begin{bmatrix} 0_{2\times 1} \\ 0_{2\times 1} \end{bmatrix}.$$

Solving for z, we get

$$z_2 = -\tilde{x}^*_2\ ;\ z_1 = (\widetilde{K}_p + K^*_p + D_\omega(\tau))^{-1}\mathcal{R} - \tilde{x}^*_1 \quad (38)$$

[2]Since A is invertible, by implicit function theorem, a solution to (23) exists.

where $\mathcal{R} = A(q)^{-1}N(q,\dot{q})$. Substituting z_1 and z_2 in (28), the quasi-steady-state value of the objective function J^i_{qs} is given by

$$J^i_{qs} = w^i_{err} \cdot \|z_1 + \tilde{x}^*_1\|^2 + \frac{w^i_{dcmf}}{(\widehat{K}_{p_i} + a\sin(\omega_i t) - \bar{K}_{p_i})^2} \quad (39)$$

$$= w^i_{err} \cdot \|(\widehat{K}_{p_i} + a\sin(\omega_i t))^{-1}\mathcal{R}\|^2 + \frac{w^i_{dcmf}}{(\widehat{K}_{p_i} + a\sin(\omega_i t) - \bar{K}_{p_i})^2} \quad (40)$$

It can be seen that the quasi-steady-state value of the objective function is independent of the damping gains K_{d_i}. ∎

Remark 4: *It can be easily shown that if the objective function had been chosen as $y^2 + \dot{y}^2$, the quasi-steady-state value of the objective function J_{qs} would have still been independent of K_d.*

In quasi-steady-state, the fast states z settle down at the equilibrium point $z = 0$, and the reduced order model is given by

$$\frac{d\widetilde{K}_{p_i}}{d\tau} = \delta K a J^i_{qs}(\widetilde{K}_{p_i} + K^*_{p_i} + a\sin\tau)\sin\tau. \quad (41)$$

Next, we prove the stability of the reduced order model (41) and the boundary layer model (obtained by taking the time-derivative of (30)) of a powered prosthetic leg with a continuous-phase controller. To proceed further, we make the following assumption on the cost function, which was verified in Section III-B.

Assumption 2: *For every walking speed, there exists a unique optimum proportional gain $K^*_{p_i}$ for the i^{th} joint, such that*

$$J^{i'}_{qs}(K^*_{p_i}) = 0\ ,\ J^{i''}_{qs}(K^*_{p_i}) > 0. \quad (42)$$

Furthermore, since J(·) is a convex function, it satisfies

$$J^{i'}_{qs}(\widetilde{K}_{p_i} + K^*_{p_i})\widetilde{K}_{p_i} > 0,\ \forall \widetilde{K}_{p_i} \neq 0 \quad (43)$$

where $J^{i'}_{qs} = \dfrac{\partial J^i_{qs}}{\partial K_{p_i}}$ and $J^{i''}_{qs} = \dfrac{\partial^2 J^i_{qs}}{\partial K^2_{p_i}}$.

Proposition 2: *Consider the closed loop feedback system (26) along with the ESC update law (27) under Assumptions 1, 2. Then there exists a small constant $\bar{\omega} > 0$ such that for every $\omega \in (0, \bar{\omega})$, the origin of the reduced order model (41) and the boundary layer model $\dot{z} = \tilde{A}(\tilde{x}, \widetilde{K}_p)\tilde{x} - \tilde{A}(\tilde{x}^*, \widetilde{K}^*_p)\tilde{x}^*$ are locally asymptotically stable.*

Proof. The first order Taylor series expansion of J^i_{qs} is given by

$$J^i_{qs}(\widetilde{K}_{p_i} + K^*_{p_i} + a\sin\tau) = J^i_{qs}(\widetilde{K}_{p_i} + K^*_{p_i}) + J^{i'}_{qs}(\widetilde{K}_{p_i} + K^*_{p_i})a\sin\tau \quad (44)$$

Using the Taylor series expansion of J^i_{qs} in (41), we have

$$\frac{d\widetilde{K}_{p_i}}{d\tau} = \delta K a(J^i_{qs}(\widetilde{K}_{p_i} + K^*_{p_i}) + J^{i'}_{qs}(\widetilde{K}_{p_i} + K^*_{p_i})a\sin\tau)\sin\tau \quad (45)$$

which is in a standard averaging form [37, Chapter 10] and thus, averaging theory can be applied. The averaged dynamics of (45) is

$$\frac{d\widetilde{K}_{p_i}}{d\tau} = \frac{\delta K a^2 J^{i'}_{qs}(\widetilde{K}_{p_i} + K^*_{p_i})}{2}. \quad (46)$$

In order to satisfy $kJ^{i''}_{qs} < 0$, a negative integrator gain is chosen, i.e., $K < 0$. Taking the derivative of Lyapunov function $V = \frac{1}{2}\widetilde{K}^2_{p_i}$ with respect to τ, we get

$$\frac{dV}{d\tau} = \frac{\delta K a^2 J^{i'}_{qs}(\widetilde{K}_{p_i} + K^*_{p_i})\widetilde{K}_{p_i}}{2} < 0 \tag{47}$$

due to Assumption 2. This proves that the reduced order system is locally asymptotically stable.

Now we perform a boundary layer model analysis. Taking the time derivative of (30), we get

$$\begin{aligned} \dot{z} &= \dot{\tilde{x}} - \dot{\tilde{x}}^* = \tilde{A}(\tilde{x}, \widetilde{K}_p)\tilde{x} + \widetilde{N}(q, \dot{q}) \\ &= \tilde{A}(\tilde{x}, \widetilde{K}_p)\tilde{x} - \tilde{A}(\tilde{x}^*, \widetilde{K}_p)\tilde{x}^* \end{aligned} \tag{48}$$

where $\widetilde{N}(q, \dot{q}) = -\tilde{A}(\tilde{x}^*, \widetilde{K}_p)\tilde{x}^*$ from (31). Equation (48) can be written in terms of z as

$$\dot{z} = \tilde{A}(z + \tilde{x}^*, \widetilde{K}_p)z + [\tilde{A}(z + \tilde{x}^*, \widetilde{K}_p) - \tilde{A}(\tilde{x}^*, \widetilde{K}_p)]\tilde{x}^*. \tag{49}$$

The first order Taylor series expansion of the right hand side of (49) about $z = 0$ is

$$\begin{aligned} \dot{z} = \Big(\frac{d}{dz}\tilde{A}(z + \tilde{x}^*, \widetilde{K}_p)z\Big|_{z=0}\Big)z + \Big[\tilde{A}(\tilde{x}^*, \widetilde{K}_p) + \\ \frac{d}{dz}\tilde{A}(z + \tilde{x}^*, \widetilde{K}_p)z\Big|_{z=0} - \tilde{A}(\tilde{x}^*, \widetilde{K}_p)\Big]\tilde{x}^* \end{aligned} \tag{50}$$

which can be shown to be

$$\dot{z} = \Big(\frac{d}{dz}\tilde{A}(z + \tilde{x}^*, \widetilde{K}_p)z\Big|_{z=0}\Big)z = \tilde{A}(\tilde{x}^*, \widetilde{K}_p)z. \tag{51}$$

Since $A(q)$ is positive definite (from Assumption 1), $\tilde{A}(\tilde{x}^*, \widetilde{K}_p)$ is negative definite, proving the boundary layer model to be locally asymptotically stable. Using Theorem 11.1 in [37] concludes the proof. ■

IV. Experimental Validation

In this section, we present the benchtop and walking experimental results to demonstrate the effectiveness of ESC for simultaneously tuning the proportional gains K_{p_i} for both of the prosthetic leg joints across different walking speeds.

A. Benchtop ESC Experiments

The tracking error profile in walking experiments can vary depending on human factors such as varying step length, muscle fatigue, foot scuffing, amongst others. Therefore, we performed benchtop experiments, which provides a controlled means of demonstrating the effectiveness of ESC adaptation results by eliminating the human factors. Since there were no external disturbances affecting the tracking error profile in the benchtop mode, the convergence of K_{p_i} could be clearly noticed. A supplemental video of one of the benchtop tests is available for download.

*1) **Different initial conditions and convex weights**:* Four benchtop tests were performed at a particular walking speed, illustrating simultaneous K_{p_i} adaptation. The prosthetic leg joints were commanded time-based knee and ankle trajectories with a period of 2 seconds. In the first two experiments, the weights on the objective functions were fixed and the initial conditions were varied to experimentally verify the convexity of the cost function. Figs. 7a, 7b show the proportional gain

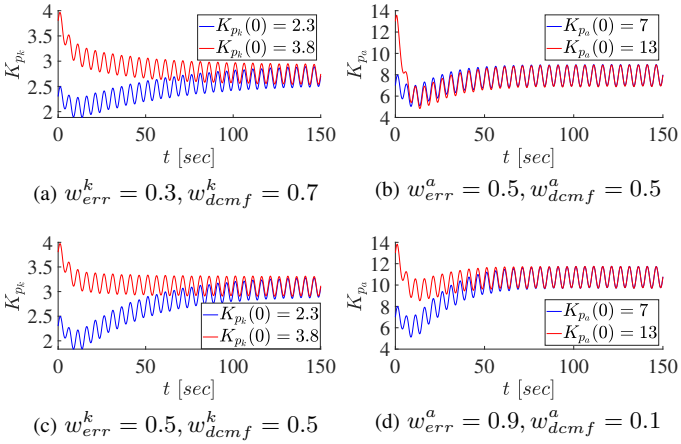

(a) $w^k_{err} = 0.3, w^k_{dcmf} = 0.7$ (b) $w^a_{err} = 0.5, w^a_{dcmf} = 0.5$

(c) $w^k_{err} = 0.5, w^k_{dcmf} = 0.5$ (d) $w^a_{err} = 0.9, w^a_{dcmf} = 0.1$

Fig. 7: Simultaneous ESC adaptation of K_{p_k} and K_{p_a}, starting from different initial conditions and different convex combinations of objective functions. The convergence to the same optimum $K^*_{p_i}$, starting from different initial K_{p_i} experimentally verified the convexity of the cost function, developed in Section III-B. Also, it can be seen that when J^i_{err} was weighed higher, K_{p_i} converged to a higher value.

adaptation results of the knee and the ankle joints, respectively, with $w^k_{err} = 0.3$, $w^a_{err} = 0.5$. In the first experiment (see the blue graphs in Figs. 7a, 7b), the initial conditions were set to $K_{p_k}(0) = 2.3$, $K_{p_a}(0) = 7$. In the second experiment (see the red graphs of Figs. 7a, 7b), the weights on the objective functions were unaltered, but the initial conditions were changed to $K_{p_k}(0) = 3.8$ and $K_{p_a}(0) = 13$. It can be noticed from Figs. 7a, 7b that the proportional gains converged to the same values, which experimentally verified the convexity of the objective function.

Next for the same set of initial conditions, another two experiments were done with higher weights on the objective function. Figs. 7c, 7d depict the adaptation results of the proportional gains for the knee and the ankle joint, respectively with $w^k_{err} = 0.5$, $w^a_{err} = 0.9$. These proportional gains correspond to higher weights on the objective functions compared to Figs. 7a, 7b. It can be noticed that if the objective function $J^i_{err,ss}$ was weighed higher than J^i_{dcmf}, K_{p_i} converges closer to $\bar{K}_{p_i}$. It is remarked that the rate of convergence for a particular joint is not affected by the weights on the objective functions.

Further results for the case presented in Figs. 7a, 7b are shown in Fig. 8. Fig. 8 shows the plot of the objective functions, $J^i_{err,ss}, J^i_{dcmf}$, $J^i_{cvx,ss}$ and the proportional gain K_{p_i} for the knee and the ankle joints. It can be seen from Figs. 8a, 8c that when K_{p_k} was initialized closer to $\bar{K}_{p_k}$, J^k_{dcmf} was initially high. When the error objective function was weighed less, i.e., $w^k_{err} = 0.3$, ESC gradually reduced K_{p_k} to minimize J^k_{dcmf}. Similarly, for the ankle joint, when $w^a_{err} = 0.5$ and $K_{p_a}(0) = 7$ (far from $\bar{K}_{p_a}$), ESC increased K_{p_a}, thereby reducing $J^a_{err,ss}$. This can be noticed for the ankle in Figs. 8b and 8d.

*2) **Trajectories with different rates of change**:* For fixed initial conditions of K_{p_i} and weights w^i_{err}, ESC was run to adapt K_{p_i} for different speeds. In particular, the initial condition of K_{p_k} and K_{p_a} were set to 2.3 and 7, respectively.

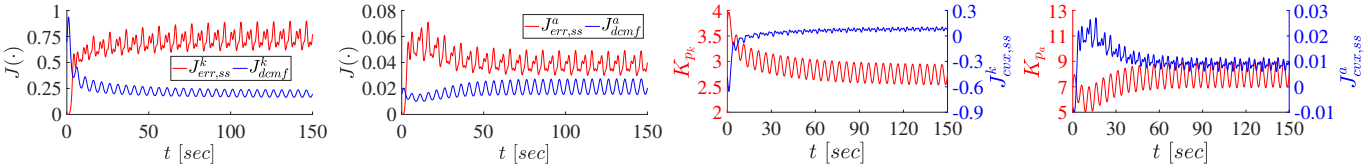

(a) Knee objective functions (b) Ankle objective functions (c) Plot of $K_{p_k}, J^k_{cvx,ss}$ (d) Plot of $K_{p_a}, J^a_{cvx,ss}$

Fig. 8: Benchtop experimental results for $w^k_{err} = 0.3, w^a_{err} = 0.5$: (a) Plot of knee objective functions, $J^k_{err,ss}$ and J^k_{dcmf}; (b) Plot of ankle objective functions, $J^a_{err,ss}$ and J^a_{dcmf}; (c) Double plot of K_{p_k} and $J^k_{cvx,ss}$; (d) Double plot of K_{p_a} and $J^a_{cvx,ss}$. As it can be seen from Figs. 8a, 8c, when initial K_{p_k} is high, i.e., $K_{p_k} = 3.8$ and J^k_{dcmf} is weighed higher, ESC reduces K_{p_k} to minimize the user's discomfort objective function J^k_{dcmf}. For the ankle joint, when the initial K_{p_a} is low, i.e., $K_{p_a} = 7$ and $J^a_{err,ss}$ is weighed higher, ESC increases K_{p_a} to minimize the tracking error objective function $J^a_{err,ss}$.

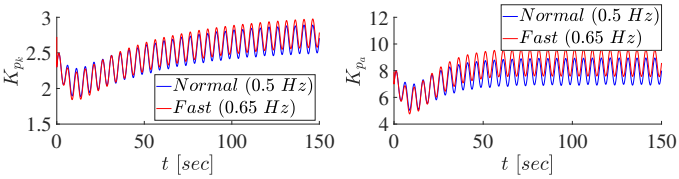

(a) $w^k_{err} = 0.3, w^k_{dcmf} = 0.7$ (b) $w^a_{err} = 0.5, w^a_{dcmf} = 0.5$

Fig. 9: Benchtop experimental results showing simultaneous ESC adaptation of K_{p_k} and K_{p_a}, for different speeds. It can be seen that K_{p_i} converges to a higher value for faster trajectories.

Two speeds of 0.5 Hz and 0.65 Hz were tested. From Fig. 6b in Section III-B, it is clear that for a given convex combination of weights on the objective functions, $J^i_{err,ss}$ and J^i_{dcmf}, the objective function $J^i_{cvx,ss}$ has different optima $K^*_{p_i}$ at different walking speeds. Fig. 9 shows simultaneous ESC adaptation of K_{p_i} at different speeds. It can be noticed that K_{p_i} for both of the joints converge to a higher value at faster speeds, which is in agreement with Fig. 6b.

B. Walking ESC Experiments

The experiment protocol used for performing walking ESC experiments is described in Appendix B. The gait tiles for slow and fast walking ESC experiments are shown in Fig. 10. Fig. 11 shows the online adaptation of K_{p_i} for different walking speeds. For all of the walking experiments, $w^k_{err} = 0.5$ and $w^a_{err} = 0.7$ were chosen. For slow walking, K_{p_k} and K_{p_a} were initialized at 3 and 7, respectively (see Fig. 11a, 11b). On starting ESC at 0.89 m/s walking speed, it was noted that K_{p_i} gradually starts increasing. At $t = 50s$, when the walking speed is changed to 1.34 m/s, the adaptation rate changes and K_{p_i} starts increasing, while the ESC algorithm starts seeking for a new optimum, which is higher for faster walking. The trend of K_{p_i} adaptation is exactly in accordance with our explanation in Section III-B. In order to verify that ESC automatically adapts to changes in walking speed, we performed another two trials by starting from fast speed and transitioned to slow speed after 50 seconds. For these trials, since the optimum for the fast walking speed is higher, K_{p_k} and K_{p_a} were initialized at 3.5 and 10, respectively. After the transient phase of ESC filters (see Figs. 11c, 11d), K_{p_i} starts increasing at faster walking speeds. At $t = 50s$, when the treadmill speed was changed to 0.89 m/s, K_{p_i} started decreasing. A supplemental video of the experiment is available for download.

Fig. 12 demonstrates a double plot of K_{p_i} and $J^i_{cvx,ss}$ for slow-to-fast and fast-to-slow walking experiments. It can be seen that when the walking speed changes from slow-to-fast, $J^i_{cvx,ss}$ increases, thereby increasing K_{p_i} (see Figs. 12a, 12b). Similarly, when the walking speed changes from fast-to-slow, $J^i_{cvx,ss}$ decreases, thereby decreasing K_{p_i} (see Figs. 12c, 12d). Although the change in the magnitude of $J^a_{cvx,ss}$ is hard to notice in Fig. 12d, an overall downward trend can be observed.

Remark 5: *A proper choice of ESC parameters is critical for stable ESC adaptation across operating conditions such as various walking speeds. We explain the procedure for selecting proper ESC parameters in Appendix A. The ESC parameter selection procedure, which is independent of the operating conditions, should be performed only once by the technician.*

V. Discussion

In this paper, we developed a convex ESC cost function that incorporated the prosthetic leg tracking error performance and the user's comfort level. In order to test the performance of ESC for simultaneously adapting the proportional gains K_{p_i} of the knee and the ankle joints, benchtop experiments were performed in order to validate the applicability of the proposed algorithm in Section III. The experimental results in Section IV were in agreement with our analysis proposed in Section III-B. In the following, we discuss the advantages and the limitations of this work.

A. Advantages of the Proposed Approach

The main challenge in automating the tuning process of control parameters of multiple joints is due to the interdependence of one joint's performance on the other. One of the main advantages of this work is that our ESC-based automatic tuning algorithm is capable of simultaneously tuning the proportional gains K_{p_i} for both of the prosthetic leg joints. This is a result of the structure of ESC, whose adaptation law for the i^{th} joint consists of filtering and demodulating operations. As a result, the ESC adaptation law isolates the effect of the other joint and computes a correlation between the i^{th} joint's performance and its proportional gain K_{p_i}. Depending on the user's preference on either the tracking

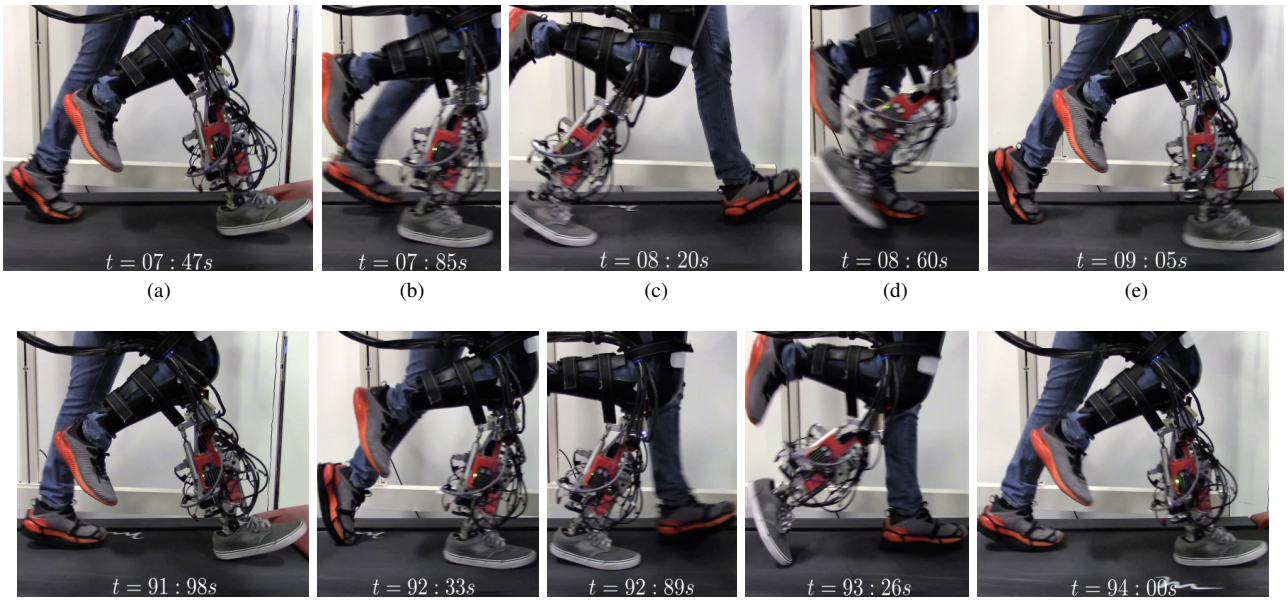

(a) (b) (c) (d) (e)

(f) (g) (h) (i) (j)

Fig. 10: Snapshots of walking experiments. Figs. 10a-10e show the photos of fast walking experiments at 1.34 m/s, and Figs. 10f-10j show the photos of slow walking experiments at 0.89 m/s for one gait cycle. A supplemental video of the experiment is available for download.

performance or the comfort factor (based on the selection of convex weights, i.e., w^i_{err}, w^i_{dcmf}), the proportional gains of the powered prosthetic leg during walking are automatically tuned by the ESC scheme. This method would eliminate the need for manual tuning of the proportional gains, which currently requires multiple iterations to achieve a balance between the prosthetic leg tracking error performance and the user's comfort.

The advantage of the continuous-phase controllers over impedance-based controllers is that the same controller can be used across different walking speeds [20], [21], at the expense of slight degradation in the tracking performance and the user's comfort level. We augment the continuous-phase controllers with our real-time ESC-based tuning algorithm that is capable of automatically changing the proportional gains K_{p_i} at different walking speeds. As compared to [6], [7], where the adaptation was shown for a particular walking speed, we demonstrated the adaptation of the control parameter K_{p_i} at different walking speeds.

Our ESC adaptation algorithm is suitably fast to react to changes in the walking speed, which is particularly attributed to the choice of the objective function used in this paper. The tracking performance of the prosthesis can be affected due to a number of factors such as walking speed and muscle fatigue, amongst others. The benchtop adaptation results in Fig. 8, 9 show that ESC takes at most 3 minutes to adapt to different walking conditions. In the walking experiments, it can be seen from Fig. 12 that the objective function changes instantly with the change in walking speed. The rapid change in the objective function enables ESC to react to the changing walking conditions and tune the proportional gains K_{p_i} accordingly. On the other hand, using a metabolic cost as an objective function leads to a very slow optimization that typically requires an hour to find an optimum [9]–[11]. Clearly, such a slow optimization process might not applicable for adapting to real-time changes in behavior or environment.

Our ESC-based adaptation algorithm does not use any off-board sensors, such as oxygen masks, in contrast to [9]–[11]. Also, we circumvented the need for expensive load cells for measuring the user's comfort by incorporating a comfort factor in the developed convex ESC cost function (see equations (15), (16)). These advantageous features of our proposed ESC algorithm makes the current approach applicable to scenarios outside the restricted lab space and inexpensive to implement.

B. Limitations

In this work, we did not investigate the effect of changing the proportional gains on the clinical aspects of amputee gait. Also, there is no guarantee that our optimal solution is metabolically efficient. Further work needs to be done in order to determine a proper objective function that better depicts the biomechanical aspects of human walking without requiring offboard sensors.

Finally, due to the time-varying nature of the adaptation scheme, ESC dynamics were initiated after the subject achieved steady-state walking, and was stopped before the subject stopped walking. This is because when the subject stopped walking, the output of the amplitude detector, which was responsible for computing the error objective function, became zero. In such a case, ESC stopped increasing the gains as the error objective function was always zero. However, since the proportional gains were still being perturbed by a time-based dither signal, ESC kept on minimizing the discomfort objective function (15), thereby saturating the proportional gains to the lowest allowable value. Clearly, in such cases

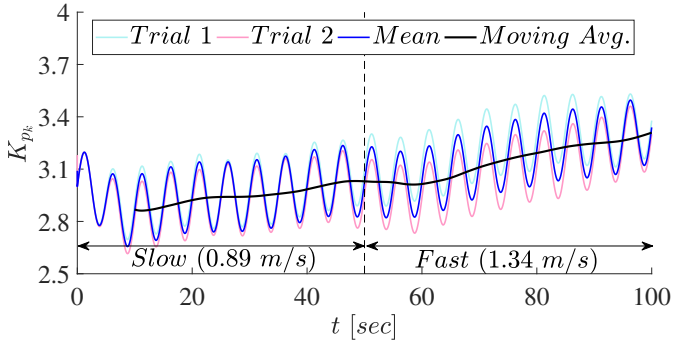

(a) K_{p_k} adaptation from slow-to-fast walking

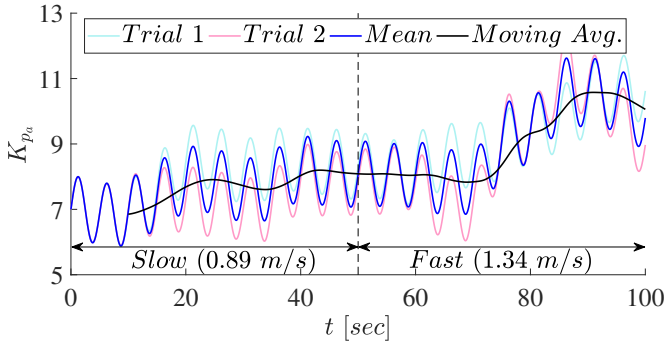

(b) K_{p_a} adaptation from slow-to-fast walking

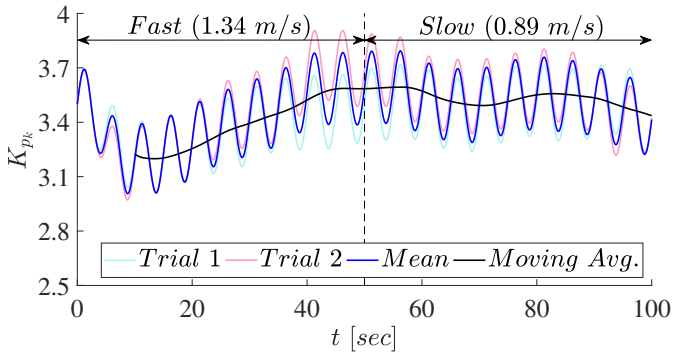

(c) K_{p_k} adaptation from fast-to-slow walking

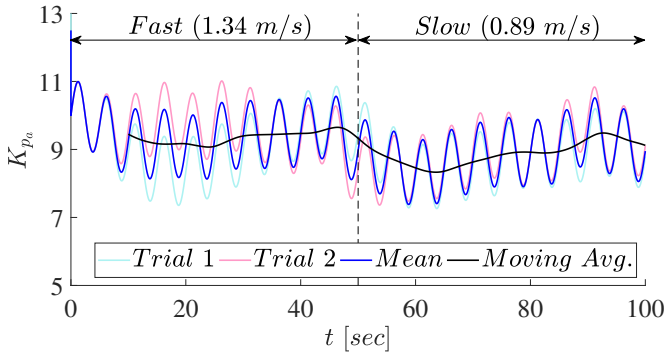

(d) K_{p_a} adaptation from fast-to-slow walking

Fig. 11: Walking ESC experimental results showing adaptation at different speeds. The black line represents the moving average of the mean of two trials with a window size of 10 seconds. The dashed vertical black line represents the time instant at which the treadmill speed is changed. It can be seen from Figs. 11a, 11b that when the user transitions from slow-to-fast walking, K_{p_i} starts increasing. Similarly, it can be seen from Figs. 11c, 11d that when the user transitions from fast-to-slow walking, K_{p_i} starts decreasing.

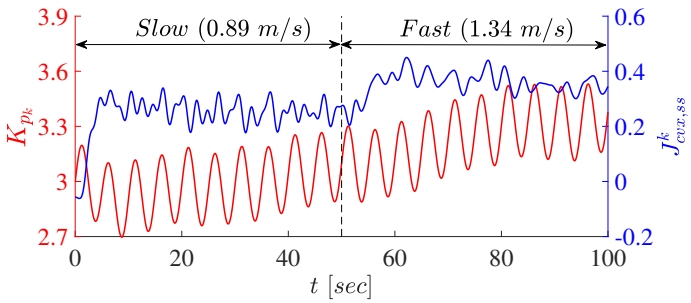

(a) K_{p_k} adaptation from slow-to-fast walking

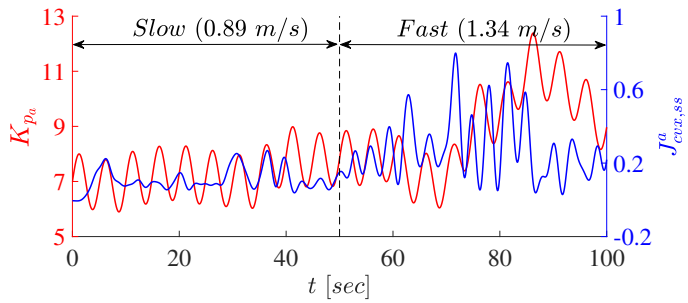

(b) K_{p_a} adaptation from slow-to-fast walking

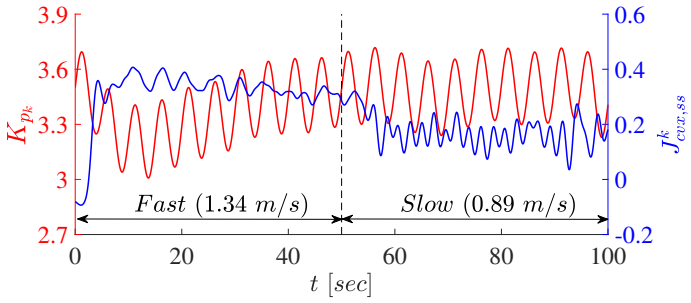

(c) K_{p_k} adaptation from fast-to-slow walking

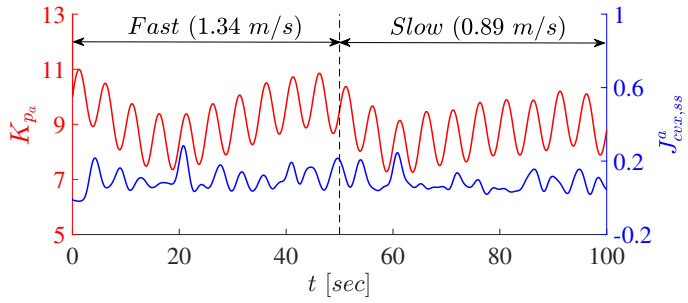

(d) K_{p_a} adaptation from fast-to-slow walking

Fig. 12: Double plot of K_{p_i} and $J^i_{cvx,ss}$ with K_{p_i} on the left y axis, shown in red and $J^i_{cvx,ss}$ on the right y axis, shown in blue. It can be seen from Figs. 12a, 12b that when the user transitions from slow-to-fast walking, the convex ESC cost function $J^i_{cvx,ss}$ increases and accordingly, ESC increases K_{p_i} for minimizing $J^i_{cvx,ss}$. Similarly, it can be seen from Figs. 12c, 12d that when the user transitions from fast-to-slow walking, $J^i_{cvx,ss}$ reduces and accordingly, ESC reduces K_{p_i} in order to minimize the user's discomfort J^i_{dcmf}.

a time-invariant ESC, i.e., independent of time-based dither signals, is needed to address such situations.

C. Clinical Application of ESC Based Auto-Tuning

The method proposed in this paper can be used to automate the tuning process of the control parameters of the prosthetic leg in a clinical setting. The selection of the ESC parameters are specific to the hardware and not the user. Therefore, the tuning of ESC parameters needs to be performed just once for each unique hardware configuration (see Remark 5). In this section, we describe the method for choosing the weights on the objective function for a particular user.

Consider a practical situation of a technician fitting a powered prosthesis to a subject. After the prosthesis is fitted to the subject, they would be instructed to walk at a slow speed (0.89 m/s) on the treadmill. While the subject walks, the proportional gains would be gradually increased by a technician until the user complains about the discomfort caused by forceful interaction of the leg. The maximum user-permissible value of the proportional gain for the i^{th} joint is recorded and denoted by $\bar{K}_{p_i}$. If the user is comfortable with proportional gains closer to $\bar{K}_{p_i}$, $w_{dcmf} \leq 0.5$ should be selected. Otherwise, $w_{dcmf} > 0.5$ should be selected so that ESC tunes the proportional gains to minimize the discomfort level of the user. *This upfront tuning process should not take more than a minute*. Once the weights on the objective functions have been tuned for a particular user, no other manual tuning needs to be performed. The proportional gains will then be automatically tuned by ESC across different walking speeds, thereby maintaining the desired preference of the user.

VI. Conclusion

This paper developed and implemented an ESC-based automatic tuning scheme for a continuous phase-based powered knee-ankle prosthetic control system. A convex objective function was built from an extensive set of fixed-gain benchtop and walking experiments, carried out at different walking speeds. A theoretical analysis was presented, which shows that the quasi-steady-state value of the objective function for continuous-phase controlled powered prosthetic legs is independent of the damping gains K_d. The advantage of the proposed method is that it relies only on the onboard sensors and does not require the knowledge of the user or prosthetic leg. The benchtop and walking experiments carried out at different speeds illustrate the strength of ESC for simultaneous adaptation of the proportional gains. Future work aims toward developing a time-invariant framework for ESC by using periodic states of the prosthetic leg as the dither signal instead of an exogenous time-based signal.

Appendix

A. Selection of ESC Parameters

According to the stability proof of ESC for general nonlinear dynamical systems in [23], the ESC parameters, i.e., $a, k, \omega, \omega_h, \omega_l$ must be chosen to be sufficiently small and depends on the closed-loop dynamics of the system. The choice of ESC parameters is carried according to what follows.

*1) **Choice of ESC dither amplitude and ESC integrator gain**:* The selection of ESC parameters, a, k, depends on the sensitivity of the system to the changes in the tunable parameters [23]. The sensitivity of the prosthetic leg joints to the changes in the proportional gains K_{p_i} can be observed from fixed-gain experiment results, explained in Section III-B. The sensitivity of the i^{th} joint to changes in K_{p_i} at a particular walking speed, denoted by $S^i_{K_p}$ can be approximated by

$$S^i_{K_p} \approx \frac{\bar{y}_i^{max} - \bar{y}_i^{min}}{K_{p_i}^{max} - K_{p_i}^{min}} \tag{52}$$

where $\bar{y}_i^{max}, \bar{y}_i^{min}$ are the maximum and minimum average filtered tracking error observed in fixed-gain experiments at a particular speed. In particular, for fast walking fixed-gain experiment, the knee and the ankle joints have sensitivities

$$S^k_{K_p} \approx \frac{\text{12.26-6.17}}{\text{5-1.8}} = 1.9 \; ; S^a_{K_p} \approx \frac{\text{0.27-0.19}}{\text{14-8}} = 0.013. \tag{53}$$

From (53), it can be noticed that the knee joint tracking error is more sensitive to the changes in K_{p_k}, as compared to the ankle. Since the ESC update law in (12) updates K_{p_i} based on the sensitivity of the joint tracking error with respect to changes in K_{p_i} [23], a, k were chosen to be smaller for the knee joint compared to the ankle. On the other hand, due to low sensitivity of the ankle tracking error to K_{p_a}, and shallow gradient of the objective function with respect to K_{p_a}, the ankle joint ESC parameters were chosen to be relatively high. The ESC parameters for both the joints are given in Table I.

Remark 6: *In order to prevent frequent oscillations between the forceful and the compliant interaction of the prosthesis with the user, small ESC parameters were selected for the knee joint.*

*2) **Choice of ESC dither frequency, HPF cut-off frequency, and LPF cut-off frequency**:* In a perturbation-based ESC, the closed loop system dynamics in (11) must be faster than the rate of change of controller parameters. In a powered prosthetic leg, we are concerned with position control. Therefore, we must ensure that the error dynamics for the i^{th} joint is much faster with respect to changes in K_{p_i}. Once the speed of the error dynamics is determined, the dither frequency must be selected to be lower than the speed of error dynamics so as to maintain a time scale separation between the error dynamics and the ESC dynamics. A procedure similar to [38] was followed to measure the speed of the error dynamics with respect to K_{p_i}. To measure the speed of the error dynamics for the i^{th} joint, step experiments were performed separately for each joint. For each joint, a step signal of 5 degrees was commanded with K_{p_i} set to the lowest allowable value. Once the steady-state error was achieved, K_{p_i} was given a step change to its highest allowable value, and the settling time was noted. Fig. 13 shows the tracking error plot for a step change in K_{p_k} and K_{p_a}. The settling time for the knee joint tracking error, y_k, and the ankle joint tracking error, y_a, are 0.6 and 0.2 seconds, respectively. Thus, the speed of the knee and the ankle error dynamics are $1/0.6 = 1.66$ Hz and $1/0.2 = 5$ Hz, respectively. Since both of the knee and the ankle joints have independent ESC loops, the same dither frequency can be used for both of the joints. From the step

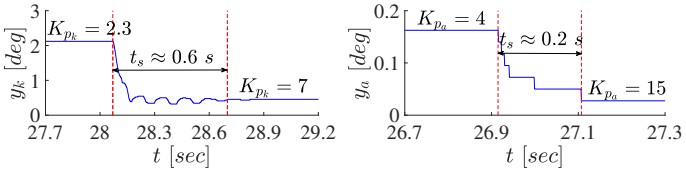

(a) Knee tracking error response (b) Ankle tracking error response

Fig. 13: Error response of the prosthetic leg joints to a step change of K_{p_i}.

TABLE I: ESC Parameters for Different Joints

ESC Parameters	Knee	Ankle
a	0.2	1
$f = \omega/2\pi$	0.2 Hz	0.2 Hz
k	-5	-60
$f_h = \omega_h/2\pi$	0.1 Hz	0.1 Hz
$f_l = \omega_l/2\pi$	0.05 Hz	0.05 Hz

experiments, we know that ω for the knee and the ankle joint should be selected to be much smaller than 1.66 Hz and 5 Hz, respectively. Furthermore, ω should also be selected smaller than the limit cycle frequency. In human walking, the subject's cadence represents the walking limit cycle frequency. The cadence, expressed in steps/minute, is related to the walking speed (m/s) and stride length (m) according to [33]

$$\text{Walking speed} = \frac{\text{Stride Length} \times \text{Cadence}}{120}. \tag{54}$$

With fixed walking speed and constant step lengths, the cadence can be determined. Due to the variations of the stride length from step to step, the cadence was determined in the following manner. First, the subject was instructed to walk on the treadmill at a particular speed with fixed K_{p_i}. After 20 seconds, when the person achieved a steady-state gait, the data logging was started. A FFT of the actual trajectory was then plotted. The FFT plots indicate that walking at 0.89 and 1.34 m/s corresponded to walking at 0.45 and 0.65 Hz, respectively. Therefore, ω was chosen as 0.2 Hz, which was slower than the plant dynamics and the limit cycle frequency. Since the filters are the slowest components of ESC, their cut-off frequencies should be selected such that $\omega_l, \omega_h \ll \omega$. A first order HPF and LPF with cut-off frequencies 0.1 and 0.05 Hz were chosen, respectively. Table I summarizes the ESC parameters used in the experiments for all the walking speeds.

B. Walking Experiment Protocol

In order to demonstrate simultaneous online adaptation of K_{p_i} to different walking speeds, two scenarios were considered. In both of the scenarios, an able-bodied subject was instructed to walk on the treadmill at a desired speed, until he achieved steady-state walking gait (walking with constant step lengths). Once the subject attained a steady-state walking gait, ESC was initiated for adapting K_{p_i}. The speed of the treadmill was changed manually around 50 seconds after the start of ESC. In the first scenario, the subject was instructed to start walking at 0.89 m/s and the treadmill speed was changed to 1.34 m/s after 50 seconds. In the second scenario, the subject was instructed to start walking at 1.34 m/s and the treadmill speed was changed to 0.89 m/s after 50 seconds. Since the tracking error varied, we performed two trials of the same scenario in order to illustrate the trend in adapting K_{p_i}.

REFERENCES

[1] N. Hogan, "Impedance control: An approach to manipulation: Part II - Implementation," *J. Dyn. Syst. Meas. Contr.*, vol. 107, no. 1, pp. 8–16, 1985.

[2] F. Sup, H. A. Varol, and M. Goldfarb, "Upslope walking with a powered knee and ankle prosthesis: initial results with an amputee subject," *IEEE Trans. Neur. Syst. Rehab. Eng.*, vol. 19, no. 1, pp. 71–78, 2011.

[3] A. Shultz, B. Lawson, and M. Goldfarb, "Running with a powered knee and ankle prosthesis," *IEEE Trans. Sys. Rehab. Eng.*, vol. 23, no. 3, pp. 403–412, 2015.

[4] B. Lawson, H. Varol, A. Huff, E. Erdemir, and M. Goldfarb, "Control of stair ascent and descent with a powered transfemoral prosthesis," *IEEE Trans. Neur. Sys. Rehab. Eng.*, vol. 21, no. 3, pp. 466–473, 2013.

[5] M. R. Tucker, J. Olivier, A. Pagel, H. Bleuler, M. Bouri, O. Lambercy, J. del R Millán, R. Riener, H. Vallery, and R. Gassert, "Control strategies for active lower extremity prosthetics and orthotics: a review," *J. Neuroeng. Rehabil.*, vol. 12, no. 1, 2015.

[6] H. Huang, D. L. Crouch, M. Liu, G. S. Sawicki, and D. Wang, "A cyber expert system for auto-tuning powered prosthesis impedance control parameters," *Annals of Biomedical Engineering*, vol. 44, no. 5, pp. 1613–1624, 2016.

[7] D. Wang, M. Liu, F. Zhang, and H. Huang, "Design of an expert system to automatically calibrate impedance control for powered knee prostheses," in *IEEE Int. Conf. Rehabil. Robot.*, 2013, pp. 1–5.

[8] Y. Wen, J. Si, X. Gao, S. Huang, and H. Huang, "A new powered lower limb prosthesis control framework based on adaptive dynamic programming," *IEEE Trans. on Neur. Net. and Learn. Sys.*, 2017.

[9] J. Zhang, P. Fiers, K. A. Witte, R. W. Jackson, K. L. Poggensee, C. G. Atkeson, and S. H. Collins, "Human-in-the-loop optimization of exoskeleton assistance during walking," *Science*, vol. 356, no. 6344, pp. 1280–1284, 2017.

[10] J. R. Koller, D. H. Gates, D. P. Ferris, and C. D. Remy, "'body-in-the-loop'optimization of assistive robotic devices: A validation study." in *Robotics: Science and Systems*, 2016.

[11] S. Lee, J. Kim, L. Baker, A. Long, N. Karavas, N. Menard, I. Galiana, and C. J. Walsh, "Autonomous multi-joint soft exosuit with augmentation-power-based control parameter tuning reduces energy cost of loaded walking," *Journal of NeuroEngineering and Rehabilitation*, vol. 15, no. 1, p. 66, Jul 2018.

[12] E. Westervelt, J. Grizzle, C. Chevallereau, J. Choi, and B. Morris, *Feedback Control of Dynamic Bipedal Robot Locomotion*. New York, NY: CRC Press, 2007.

[13] K. Sreenath, H. W. Park, I. Poulakakis, and J. W. Grizzle, "A compliant hybrid zero dynamics controller for stable, efficient and fast bipedal walking on MABEL," *Int. J. Robot. Res.*, vol. 30, no. 9, pp. 1170–1193, 2011.

[14] C. Chevallereau, G. Abba, Y. Aoustin, F. Plestan, E. R. Westervelt, C. Canudas-de-Wit, and J. W. Grizzle, "RABBIT: A testbed for advanced control theory," *IEEE Control Systems Magazine*, vol. 23, no. 5, pp. 57–79, 2003.

[15] A. M. Kohl, E. Kelasidi, A. Mohammadi, M. Maggiore, and K. Y. Pettersen, "Planar maneuvering control of underwater snake robots using virtual holonomic constraints," *Bioinspiration & Biomimetics*, vol. 11, no. 6, p. 065005, 2016.

[16] R. D. Gregg, T. Lenzi, L. J. Hargrove, and J. W. Sensinger, "Virtual constraint control of a powered prosthetic leg: From simulation to experiments with transfemoral amputees," *IEEE Trans. Robotics*, vol. 30, no. 6, pp. 1455–1471, 2014.

[17] A. E. Martin and R. D. Gregg, "Hybrid invariance and stability of a feedback linearizing controller for powered prostheses," in *2015 American Control Conference (ACC)*. IEEE, 2015, pp. 4670–4676.

[18] ——, "Stable, robust hybrid zero dynamics control of powered lower-limb prostheses," *IEEE Transactions on Automatic Control*, vol. 62, no. 8, pp. 3930–3942, Aug 2017.

[19] D. Quintero, A. E. Martin, and R. D. Gregg, "Toward unified control of a powered prosthetic leg: A simulation study," *IEEE Transactions on Control Systems Technology*, vol. 26, no. 1, pp. 305–312, Jan 2018.

[20] D. Quintero, D. J. Villarreal, and R. D. Gregg, "Preliminary experiments with a unified controller for a powered knee-ankle prosthetic leg across walking speeds," in *IEEE/RSJ Int. Conf. Intell. Robot. Syst.*, 2016, pp. 5427–5433.

[21] D. Quintero, D. J. Villarreal, D. J. Lambert, S. Kapp, and R. D. Gregg, "Continuous-phase control of a powered knee-ankle prosthesis: Amputee experiments across speeds and inclines," *IEEE Transactions on Robotics*, vol. 34, no. 3, pp. 686–701, June 2018.

[22] Q. Nguyen and K. Sreenath, "L^1 adaptive control for bipedal robots with control lyapunov function based quadratic programs," in *American Contr. Conf.*, 2015, pp. 862–867.

[23] M. Krstić and H.-H. Wang, "Stability of extremum seeking feedback for general nonlinear dynamic systems," *Automatica*, vol. 36, no. 4, pp. 595–601, 2000.

[24] K. B. Ariyur and M. Krstic, *Real-time optimization by extremum-seeking control*. John Wiley & Sons, 2003.

[25] B. J. Hafner, L. L. Willingham, N. C. Buell, K. J. Allyn, and D. G. Smith, "Evaluation of function, performance, and preference as transfemoral amputees transition from mechanical to microprocessor control of the prosthetic knee," *Archives of physical medicine and rehabilitation*, vol. 88, no. 2, pp. 207–217, 2007.

[26] N. J. Killingsworth and M. Krstic, "Pid tuning using extremum seeking: online, model-free performance optimization," *IEEE Control Systems*, vol. 26, no. 1, pp. 70–79, Feb 2006.

[27] S. Kumar, A. Mohammadi, N. Gans, and R. D. Gregg, "Automatic tuning of virtual constraint-based control algorithms for powered knee-ankle prostheses," in *2017 IEEE Conf. on Control Tech. and App. (CCTA)*, pp. 812–818.

[28] D. Quintero, A. E. Martin, and R. D. Gregg, "Unifying the gait cycle in the control of a powered prosthetic leg," in *2015 IEEE International Conference on Rehabilitation Robotics (ICORR)*. IEEE, 2015, pp. 289–294.

[29] H.-H. Wang and M. Krstic, "Extremum seeking for limit cycle minimization," *IEEE Transactions on Automatic Control*, vol. 45, no. 12, pp. 2432–2436, 2000.

[30] Y. Tan, D. Nešić, and I. Mareels, "On non-local stability properties of extremum seeking control," *Automatica*, vol. 42, no. 6, pp. 889–903, 2006.

[31] L. Hazeleger, M. Haring, and N. van de Wouw, "Extremum-seeking control for steady-state performance optimization of nonlinear plants with time-varying steady-state outputs," *American Control Conference*, pp. 2990–2995, 2018.

[32] X. T. Zhang, D. M. Dawson, W. E. Dixon, and B. Xian, "Extremum-seeking nonlinear controllers for a human exercise machine," *IEEE/ASME Transactions on Mechatronics*, vol. 11, no. 2, pp. 233–240, April 2006.

[33] D. A. Winter, *Biomechanics and motor control of human movement*. John Wiley & Sons, 2009.

[34] J. L. Johansson, D. M. Sherrill, P. O. Riley, P. Bonato, and H. Herr, "A clinical comparison of variable-damping and mechanically passive prosthetic knee devices," *American journal of physical medicine & rehabilitation*, vol. 84, no. 8, pp. 563–575, 2005.

[35] S. Kumar and N. Gans, "Extremum seeking control for multi-objective optimization problems," in *IEEE Conf. Dec. Contr.*, 2016, pp. 1112–1118.

[36] K. T. Atta, A. Johansson, and M. Guay, "On the generalization and stability analysis of pareto seeking control," *IEEE Control Systems Letters*, vol. 2, no. 1, pp. 145–150, 2018.

[37] H. K. Khalil, "Nonlinear systems, 3rd ed." *New Jersey, Prentice Hall*, 2002.

[38] A. Banaszuk, K. B. Ariyur, M. Krstić, and C. A. Jacobson, "An adaptive algorithm for control of combustion instability," *Automatica*, vol. 40, no. 11, pp. 1965–1972, 2004.